Predicting the clinical impact of human mutation with deep neural networks

Laksshman Sundaram[1,2,3,*], **Hong Gao**[1,*], **Samskruthi Reddy Padigepati**[1,3], **Jeremy F. McRae**[1], **Yanjun Li**[3], **Jack A. Kosmicki**[1,4], **Nondas Fritzilas**[1], **Jörg Hakenberg**[1], **Anindita Dutta**[1], **John Shon**[1], **Jinbo Xu**[5], **Serafim Batzoglou**[1], **Xiaolin Li**[3], and **Kyle Kai-How Farh**[1,†]

[1]Illumina Artificial Intelligence Laboratory, Illumina Inc, San Diego, California, USA

[2]Department of Computer Science, Stanford University, Stanford, California, USA

[3]National Science Foundation Center for Big Learning, University of Florida, Gainesville, Florida, USA

[4]Analytic and Translational Genetics Unit (ATGU), Department of Medicine, Massachusetts General Hospital and Harvard Medical School, Boston Massachusetts, USA

[5]Toyota Technological Institute at Chicago, Chicago, Illinois, USA

Abstract

Millions of human genomes and exomes have been sequenced, but their clinical applications remain limited due to the difficulty of distinguishing disease-causing mutations from benign genetic variation. Here we demonstrate that common missense variants in other primate species are largely clinically benign in human, enabling pathogenic mutations to be systematically identified by process of elimination. Using hundreds of thousands of common variants from population sequencing of six non-human primate species, we train a deep neural network that identifies pathogenic mutations in rare disease patients with 88% accuracy, and enables the discovery of 14 new candidate genes in intellectual disability at genome-wide significance. Cataloging common variation from additional primate species would improve interpretation for millions of variants of uncertain significance, further advancing the clinical utility of human genome sequencing.

Introduction

The clinical actionability of diagnostic sequencing is limited by the difficulty of interpreting rare genetic variants in human populations and inferring their impact on disease risk[1,2]. Because of their deleterious effects on fitness, clinically significant genetic variants tend to be extremely rare in the population, and for the vast majority, their effects on human health have not been determined[3]. The large number and rarity of these variants of uncertain clinical significance present a formidable obstacle to the adoption of sequencing for individualized medicine and population-wide health screening[4].

Most penetrant Mendelian diseases have very low prevalence in the population, hence the observation of a variant at high frequencies in the population is strong evidence in favor of benign consequence[5]. Assaying common variation across diverse human populations is an effective strategy for cataloguing benign variants[6], but the total amount of common variation in present day humans is limited due to bottleneck events in our species' recent history, during which a large fraction of ancestral diversity was lost[7]. Population studies of present day humans show a remarkable inflation from an effective population size (N_e) of less than 10,000 individuals within the last 15,000–65,000 years, and the small pool of common polymorphisms traces back to the limited capacitance for variation in a population of this size[8]. Out of more than 70 million potential protein-altering missense substitutions in the reference genome, only roughly 1 in 1000 are present at greater than 0.1% overall population allele frequency[6,9].

Outside of modern human populations, chimpanzees comprise the next closest extant species, and share 99.4% amino acid sequence identity[10]. The near-identity of protein-coding sequence in humans and chimpanzees suggests that purifying selection operating on chimpanzee protein-coding variants might also model the consequences on fitness of human mutations that are identical-by-state. Because the mean time for neutral polymorphisms to persist in the ancestral human lineage (~$4N_e$ generations) is a fraction of the species' divergence time (~6 mya)[11], naturally occurring chimpanzee variation explores mutational space that is largely non-overlapping except by chance, aside from rare instances of haplotypes maintained by balancing selection[12,13]. If polymorphisms that are identical-by-state similarly affect fitness in the two species, the presence of a variant at high allele frequencies in chimpanzee populations should indicate benign consequence in human, expanding the catalog of known variants whose benign consequence has been established by purifying selection.

Results

Common variants in other primates are largely benign in human

The recent availability of aggregated exome data, comprising 123,136 humans collected in the Exome Aggregation Consortium (ExAC) and Genome Aggregation Database (gnomAD), allows us to measure the impact of natural selection on missense and synonymous mutations across the allele frequency spectrum[6]. Rare singleton variants that are observed only once in the cohort closely match the expected 2.2:1 missense:synonymous ratio predicted by *de novo* mutation after adjusting for the effects of trinucleotide context on

mutational rate (Fig. 1a and Supplementary Fig. 1, 2)[14], but at higher allele frequencies the number of observed missense variants decreases due to the purging of deleterious mutations by natural selection. The gradual decrease of missense:synonymous ratios with increasing allele frequency is consistent with a substantial fraction of missense variants of population frequency < 0.1% having mildly deleterious consequence despite being observed in healthy individuals[15]. These findings support the widespread empirical practice by diagnostic labs of filtering out variants with greater than 0.1%~1% allele frequency as likely benign for penetrant genetic disease, aside from a handful of well-documented exceptions due to balancing selection and founder effects[16,17].

We identified common chimpanzee variants that were sampled two or more times in a cohort of 24 unrelated individuals[18]; we estimate that 99.8% of these variants are common in the general chimpanzee population (allele frequency (AF) > 0.1%), indicating that these variants have already passed through the sieve of purifying selection (see Methods). We examined the human allele frequency spectrum for the corresponding identical-by-state human variants (Fig. 1b), excluding the extended major histocompatibility complex region as a known region of balancing selection[19], along with variants lacking a one-to-one mapping in the multiple sequence alignment. For human variants that are identical-by-state with common chimpanzee variants, the missense:synonymous ratio is largely constant across the human allele frequency spectrum ($P > 0.5$ by χ^2 test), which is consistent with absence of negative selection against common chimpanzee variants in the human population and concordant selection coefficients on missense variants in the two species. The low missense:synonymous ratio observed in human variants that are identical-by-state with common chimpanzee variants is consistent with the larger effective population size in chimpanzee ($N_e \sim 73,000$), which enables more efficient filtering of mildly deleterious variation[20,21].

In contrast, for singleton chimpanzee variants (sampled only once in the cohort), we observe a significant decrease in the missense:synonymous ratio at common allele frequencies ($P < 5.8 \times 10^{-6}$; Fig. 1c), indicating that 24% of singleton chimpanzee missense variants would be filtered by purifying selection in human populations at allele frequencies greater than 0.1%. This depletion indicates that a significant fraction of the chimpanzee singleton variants are rare deleterious mutations whose damaging effects on fitness have prevented them from reaching common allele frequencies in either species. We estimate that only 69% of singleton variants are common (AF > 0.1%) in the general chimpanzee population (see Methods).

We next identified human variants that are identical-by-state with variation observed in at least one of six non-human primate species. Variation in each of the six species was ascertained from either the great ape genome project (chimp, bonobo, gorilla, orangutan)[18] or were submitted to dbSNP from the primate genome projects (rhesus, marmoset)[22–25], and largely represent common variants based on the limited number of individuals sequenced and the low missense:synonymous ratios observed for each species (Supplementary Table 1). Similar to chimpanzee, we find that the missense:synonymous ratios for variants from the six non-human primate species are roughly equal across the human allele frequency spectrum, other than a mild depletion of missense variation at common allele frequencies

(Fig. 1d, Supplementary Fig. 3 and Supplementary Data File 1), which is expected due to the inclusion of a minority of rare variants (~16% with under 0.1% allele frequency in chimpanzee, and less in other species due to fewer individuals sequenced; see Methods and Supplementary Note). These results suggest that the selection coefficients on identical-by-state missense variants are concordant within the primate lineage at least out to new world monkeys, which are estimated to have diverged from the human ancestral lineage ~35 million years ago[26].

We find that human missense variants that are identical-by-state with observed primate variants are strongly enriched for benign consequence in the ClinVar database[27]. After excluding variants of uncertain significance and those with conflicting annotations, ClinVar variants that are present in at least one non-human primate species are annotated as Benign or Likely Benign on average 90% of the time, compared to 35% for ClinVar missense variants in general ($P < 10^{-40}$; Fig. 1e). The pathogenicity of ClinVar annotations for primate variants is slightly greater than that observed from sampling a similarly sized cohort of healthy humans (~95% Benign or Likely Benign consequence, $P = 0.07$; see Methods and Supplementary Note) excluding human variants with greater than 1% allele frequency to reduce curation bias.

The field of human genetics has long relied upon model organisms to infer the clinical impact of human mutations[28,29], but the long evolutionary distance to most genetically tractable animal models raises concerns about the extent to which findings on model organisms are generalizable back to human[30]. We extended our analysis beyond the primate lineage to include largely common variation from four additional mammalian species (mouse, pig, goat, cow) and two species of more distant vertebrates (chicken, zebrafish). We selected species with sufficient genome-wide ascertainment of variation in dbSNP, and confirmed that these are largely common variants, based on missense:synonymous ratios being much lower than 2.2:1 (see Methods and Supplementary Note). In contrast to our primate analyses, human missense mutations that are identical-by-state with variation in more distant species are markedly depleted at common allele frequencies (Fig. 2a), and the magnitude of this depletion increases at longer evolutionary distances (Fig. 2b and Supplementary Tables 2 and 3).

The missense mutations that are deleterious in human, yet tolerated at high allele frequencies in more distant species, indicate that the coefficients of selection for identical-by-state missense mutations have diverged substantially between human and more distant species. Nonetheless, the presence of a missense variant in more distant mammals still increases the likelihood of benign consequence, as the fraction of missense variants depleted by natural selection at common allele frequencies is less than the ~50% depletion observed for human missense variants in general (Fig. 1a). Consistent with these results, we find that ClinVar missense variants that have been observed in mouse, pig, goat, and cow are 73% likely to be annotated with Benign or Likely Benign consequence, compared to 90% for primate variation ($P < 2 \times 10^{-8}$; Fig. 2c), and 35% for the ClinVar database overall.

To confirm that evolutionary distance, and not domestication artifact, is the primary driving force for the divergence of the selection coefficients, we repeated the analysis using fixed

substitutions between pairs of closely related species in lieu of intra-species polymorphisms across a broad range of evolutionary distances (Fig. 2d, Supplementary Table 4 and Supplementary Data File 2). We find that the depletion of human missense variants that are identical-by-state with inter-species fixed substitutions increases with evolutionary branch length, with no discernable difference for wild species compared to those exposed to domestication. This concurs with earlier work in fly and yeast[31], which found that the number of identical-by-state fixed missense substitutions were lower than expected by chance in divergent lineages.

A deep learning network for variant pathogenicity classification

The importance of variant classification for clinical applications has inspired numerous attempts to use supervised machine learning to address the problem, but these efforts have been hindered by the lack of an adequately-sized truth dataset containing confidently labeled benign and pathogenic variants for training[32–42]. Existing databases of human expert curated variants do not represent the entire genome, with ~50% of the variants in the ClinVar database coming from only 200 genes (~1% of human protein-coding genes). Moreover, systematic studies reveal that many human expert annotations have questionable supporting evidence[6,43], underscoring the difficulty of interpreting rare variants that may be observed in only a single patient. Although human expert interpretation has become increasingly rigorous[1,5], classification guidelines are largely formulated around consensus practices, and are at risk of reinforcing existing tendencies. To reduce human interpretation biases, recent classifiers have been trained on common human polymorphisms or fixed human-chimpanzee substitutions[44–47], but these classifiers also use as their input the prediction scores of earlier classifiers that were trained on human curated databases. Objective benchmarking of the performance of these various methods has been elusive in the absence of an independent, bias-free truth dataset[48].

Variation from the six non-human primates (chimpanzee, bonobo, gorilla, orangutan, rhesus, and marmoset) contributes over 300,000 unique missense variants that are non-overlapping with common human variation, and largely represent common variants of benign consequence that have been through the sieve of purifying selection, greatly enlarging the training dataset available for machine learning approaches. On average, each primate species contributes more variants than the whole of the ClinVar database (~42,000 missense variants as of Nov 2017, after excluding variants of uncertain significance and those with conflicting annotations). Additionally, this content is free from biases in human interpretation.

Using a dataset consisting of common human variants ($AF > 0.1\%$) and primate variation (Supplementary Table 5), we trained a novel deep residual network, PrimateAI, which takes as input the amino acid sequence flanking the variant of interest and the orthologous sequence alignments in other species (Fig. 3a and Supplementary Fig. 4)[49]. Unlike existing classifiers which employ human-engineered features, our deep learning network learns to extract features directly from primary sequence. To incorporate information about protein structure, we trained separate networks to predict secondary structure and solvent accessibility from sequence alone[50,51], and then included these as sub-networks in the full model (Fig. 3b and Supplementary Fig. 5). Given the small number of human proteins that

have been successfully crystallized, inferring structure from primary sequence has the advantage of avoiding biases due to incomplete protein structure and functional domain annotation. The total depth of the network, with protein structure included, was 36 layers of convolutions, consisting of roughly 400,000 trainable parameters.

To train a classifier using only variants with benign labels, we framed the prediction problem as whether a given mutation is likely to be observed as a common variant in the population. Several factors influence the probability of observing a variant at high allele frequencies, of which we are interested only in deleteriousness; other factors include mutation rate, technical artifacts such as sequencing coverage, and factors impacting neutral genetic drift such as gene conversion[52]. We matched each variant in the benign training set with a missense mutation that was absent in 123,136 exomes from the ExAC database, controlling for each of these confounding factors, and trained the deep learning network to distinguish between benign variants and matched controls (Supplementary Fig. 6)[14]. As the number of unlabeled variants greatly exceeds the size of the labeled benign training dataset, we trained eight networks in parallel, each using a different set of unlabeled variants matched to the benign training dataset, to obtain a consensus prediction.

Using only primary amino acid sequence as its input, the deep learning network accurately assigns high pathogenicity scores to residues at critical protein functional domains, as shown for the voltage-gated sodium channel SCN2A (Fig. 3c), a major disease gene in epilepsy, autism, and intellectual disability. The structure of the SCN2A consists of four homologous repeats, each containing six transmembrane helixes (S1–S6)[53,54]. Upon membrane depolarization, the positively-charged S4 transmembrane helix moves towards the extracellular side of the membrane, causing the S5/S6 pore-forming domains to open via the S4–S5 linker. Mutations in the S4, S4–S5 linker, and S5 domains, which are clinically associated with early onset epileptic encephalopathy[55], are predicted by the network to have the highest pathogenicity scores in the gene, and are depleted for variants in the healthy population (Supplementary Table 6). We also find that the network recognizes important amino acid positions within domains, and assigns the highest pathogenicity scores to mutations at these positions, such as the DNA-contacting residues of transcription factors and the catalytic residues of enzymes (Supplementary Fig. 7). To better understand how the deep learning network derives insights into protein structure and function from primary sequence, we visualized the trainable parameters from the first three layers of the network. Within these layers, we observe that the network learns correlations between the weights of different amino acids which approximate existing measurements of amino acid distance such as Grantham score (Supplementary Fig. 8)[56–58]. The outputs of these initial layers become the inputs for later layers, enabling the deep learning network to construct progressively higher order representations of the data[59].

We compared the performance of our network with existing classification algorithms, using 10,000 common primate variants that were withheld from training (Supplemental Data File 3). Because ~50% of all newly arising human missense variants are filtered by purifying selection at common allele frequencies (Fig. 1a), we determined the 50th-percentile score for each classifier using randomly selected variants that were matched to the 10,000 common primate variants by mutational rate and sequencing coverage, and evaluated the

accuracy of each classifier at that threshold (Fig. 3d, Supplementary Fig. 9a and Supplemental Data File 4). Our deep learning network (91% accuracy) surpassed the performance of other classifiers (80% accuracy for the next best model) at assigning benign consequence to the 10,000 withheld common primate variants. Roughly half the improvement over existing methods comes from using the deep learning network, and half comes from augmenting the training dataset with primate variation, as compared to the accuracy of the network trained with human variation data only (Fig. 3d).

To test classification of variants of uncertain significance in a clinical scenario, we evaluated the ability of the deep learning network to distinguish between *de novo* mutations occurring in patients with neurodevelopmental disorders versus healthy controls. By prevalence, neurodevelopmental disorders constitute one of the largest categories of rare genetic diseases[60], and recent trio sequencing studies have implicated the central role of *de novo* missense and protein truncating mutations[61–64]. We classified each confidently called *de novo* missense variant in 4,293 affected individuals from the Deciphering Developmental Disorders cohort (DDD)[65], versus *de novo* missense variants from 2,517 unaffected siblings in the Simon's Simplex Collection cohort (SSC)[66], and assessed the difference in prediction scores between the two distributions with the Wilcoxon rank-sum test (Fig. 3e and Supplementary Fig. 10). The deep learning network clearly outperforms other classifiers on this task ($P < 10^{-28}$; Fig. 3f and Supplementary Fig. 9b). Moreover, the performance of the various classifiers on the withheld primate variant dataset and the DDD cases vs controls dataset were correlated (Spearman $\rho = 0.57$, $P < 0.01$), indicating good agreement between the two datasets for evaluating pathogenicity, despite using entirely different sources and methodologies (Supplementary Fig. 11a).

We next sought to estimate the accuracy of the deep learning network at classifying benign versus pathogenic mutations within the same gene. Given that the DDD population largely consists of index cases of affected children without affected first degree relatives, it is essential to show that the classifier has not inflated its accuracy by favoring pathogenicity in genes with *de novo* dominant modes of inheritance. We restricted the analysis to 605 genes that were nominally significant for disease association in the DDD study, calculated from protein-truncating variation only ($P < 0.05$)[65]. Within these genes, *de novo* missense mutations are enriched 3:1 compared to expectation (Fig. 4a), indicating that ~67% are pathogenic. The deep learning network was able to discriminate pathogenic and benign *de novo* variants within the same set of genes ($P < 10^{-15}$; Fig. 4b), outperforming other methods by a large margin (Fig. 4c and Supplementary Fig. 9c). At a binary cutoff of 0.803 (Fig. 4d and Supplementary Fig. 11b), 65% of *de novo* missense mutations in cases are classified by the deep learning network as pathogenic, compared to 14% of *de novo* missense mutations in controls, corresponding to a classification accuracy of 88% (Fig. 4e and Supplementary Fig. 11c). Given frequent incomplete penetrance and variable expressivity in neurodevelopmental disorders[67], this figure likely underestimates the accuracy of our classifier due to the inclusion of partially penetrant pathogenic variants in controls. We caution that data from a greater diversity of disease genes are needed before generalizing these conclusions out to all Mendelian disorders.

Novel candidate gene discovery

Applying a threshold of 0.803 to stratify pathogenic missense mutations increases the enrichment of *de novo* missense mutations in DDD patients from 1.5-fold to 2.2-fold, close to protein-truncating mutations (2.5-fold), while relinquishing less than one third of the total number of variants enriched above expectation. This substantially improves statistical power, enabling discovery of 14 additional candidate genes in intellectual disability, which had previously not reached the genome-wide significance threshold in the original DDD study (Table 1). Additional clinical validation will be necessary to confirm these candidates and understand the spectrum of their genotype-phenotype relationships.

Comparison with human expert curation

We examined the performance of various classifiers on recent human expert-curated variants from the ClinVar database, but find that the performance of classifiers on the ClinVar dataset was not significantly correlated with either the withheld primate variant dataset or the DDD case vs control dataset ($P = 0.12$ and $P = 0.34$, respectively) (Supplementary Fig. 12). We hypothesize that existing classifiers have biases from human expert curation, and while these human heuristics tend to be in the right direction, they may not be optimal. One example is the mean difference in Grantham score between pathogenic and benign variants in ClinVar, which is twice as large as the difference between *de novo* variants in DDD cases versus controls within the 605 disease-associated genes (Table 2). In comparison, human expert curation appears to underutilize protein structure, especially the importance of the residue being exposed at the surface where it can be available to interact with other molecules. We observe that both ClinVar pathogenic mutations and DDD *de novo* mutations are associated with predicted solvent-exposed residues, but that the difference in solvent accessibility between benign and pathogenic ClinVar variants is only half that seen for DDD cases versus controls. These findings are suggestive of ascertainment bias in favor of factors that are more straightforward for a human expert to interpret, such as Grantham score and conservation. Machine learning classifiers trained on human curated databases would be expected to reinforce these tendencies.

Discussion

Our results suggest that systematic primate population sequencing is an effective strategy to classify the millions of human variants of uncertain significance that currently limit clinical genome interpretation. The accuracy of our deep learning network on both withheld common primate variants and clinical variants increases with the number of benign variants used to train the network (Fig. 5a). Moreover, training on variants from each of the six non-human primate species independently contributes to increasing the performance of the network (Fig. 5b, c), whereas training on variants from more distant mammals negatively impacts the performance of the network. These results support the assertion that common primate variants are largely benign in human with respect to penetrant Mendelian disease, while the same cannot be said of variation in more distant species.

Although the number of non-human primate genomes examined in this study is small compared to the number of human genomes and exomes that have been sequenced, it is

important to note that these additional primates contribute a disproportionate amount of information about common benign variation. Simulations with ExAC show that discovery of common human variants (>0.1% allele frequency) plateaus quickly after only a few hundred individuals (Supplementary Fig. 13), and further healthy population sequencing into the millions mainly contributes additional rare variants. Unlike common variants, which are known to be largely clinically benign based on allele frequency, rare variants in healthy populations may cause recessive genetic diseases or dominant genetic diseases with incomplete penetrance. Because each primate species carries a different pool of common variants, sequencing several dozen members of each species is an effective strategy to systematically catalog benign missense variation in the primate lineage. Indeed, the 134 individuals from six non-human primate species examined in this study contribute nearly four times as many common missense variants as the 123,136 humans from the ExAC study (Supplementary Table 5). Primate population sequencing studies involving hundreds of individuals may be practical even with the relatively small numbers of unrelated individuals residing in wildlife sanctuaries and zoos, thus minimizing the disturbance to wild populations, which is important from the standpoint of conservation and ethical treatment of non-human primates.

Present day human populations carry much lower genetic diversity than most non-human primate species[68], with roughly half the number of single nucleotide variants per individual as chimpanzee, gorilla, and gibbon, and 1/3 as many variants per individual as orangutan[18]. Although genetic diversity levels for the majority of non-human primate species are not known, the large number of extant non-human primate species allows us to extrapolate that the majority of possible benign human missense positions are likely to be covered by a common variant in at least one primate species, enabling pathogenic variants to be systematically identified by process of elimination (Fig. 5d). Even with only a subset of these species sequenced, increasing the training data size will enable more accurate prediction of missense consequence with machine learning. Finally, while our findings in this paper focus on missense variation, this strategy may also be applicable for inferring the consequences of noncoding variation, particularly in conserved regulatory regions where there is sufficient alignment between human and primate genomes to unambiguously determine whether a variant is identical-by-state.

Of the 504 known non-human primate species, roughly 60% face extinction due to poaching and widespread habitat loss[69]. The reduction in population size and potential extinction of these species represents an irreplaceable loss in genetic diversity, motivating urgency for a worldwide conservation effort that would benefit both these unique and irreplaceable species and our own.

Online Methods

Data generation and alignment

Coordinates in the paper refer to human genome build UCSC hg19/GRCh37, including the coordinates for variants in other species mapped to hg19 using multiple sequence alignments. Canonical transcripts for protein-coding DNA sequence and multiple sequence

alignments of 99 vertebrate genomes and branch length were downloaded from the UCSC genome browser[70,71](see URLs).

We obtained human exome polymorphism data from the Exome Aggregation Consortium (ExAC)/genome Aggregation Database (gnomAD exomes) v2.0[6] (see URLs). We obtained primate variation data from the great ape genome sequencing project[18], which consisted of whole genome sequencing data and genotypes for 24 chimpanzees, 13 bonobos, 27 gorillas and 10 orangutans. We also included variation from 35 chimpanzees from a separate study of chimpanzee and bonobos[21], but due to differences in variant calling methodology, we excluded these from the population analysis, and used them only for training the deep learning model. In addition, 16 rhesus individuals and 9 marmoset individuals were used to assay variation in the original genome projects for these species, but individual-level information was not available[23,24]. We obtained variation data for rhesus, marmoset, pig, cow, goat, mouse, chicken, and zebrafish from dbSNP[25]. dbSNP also included additional orangutan variants, which we only used for training the deep learning model, since individual genotype information was not available for the population analysis. To avoid effects due to balancing selection, we also excluded variants from within the extended MHC region (chr6: 28,477,797–33,448,354) for the population analysis.

We used the multiple species alignment of 99 vertebrates to ensure orthologous 1:1 mapping to human protein-coding regions and prevent mapping to pseudogenes. We accepted variants as identical-by-state if they occurred in either reference/alternative orientation. To ensure that the variant had the same predicted protein-coding consequence in both human and the other species, we required that the other two nucleotides in the codon are identical between the species, for both missense and synonymous variants. Polymorphisms from each species included in the analysis are listed in Supplementary Data File 1 and detailed metrics are shown in Supplementary Table 1.

For each of the four allele frequency categories (Fig. 1a), we used intronic sequence to estimate the expected number of synonymous and missense variants in each of 96 possible tri-nucleotide contexts and correct for mutational rate (Supplementary Fig. 1 and Supplementary Tables 7,8). We also separately analyzed identical-by-state CpG and non-CpG variants, and verified that the missense: synonymous ratio was flat across the allele frequency spectrum for both classes, indicating that our analysis holds for both CpG and non-CpG variants, despite the large difference in their mutation rate (Supplementary Fig. 2 and Supplementary Note).

Depletion of human missense variants that are identical-by-state with polymorphisms in other species

To evaluate whether variants present in other species would be tolerated at common allele frequencies (> 0.1%) in human, we identified human variants that were identical-by-state with variation in the other species. For each of the variants, we assigned them to one of the four categories based on their allele frequencies in human populations (singleton, more than singleton~0.01%, 0.01%~0.1%, > 0.1%), and estimated the decrease in missense: synonymous ratios (MSR) between the rare (< 0.1%) and common (> 0.1%) variants. The depletion of identical-by-state missense variants at common human allele frequencies (>

0.1%) indicates the fraction of variants from the other species that are sufficiently deleterious that they would be filtered out by natural selection at common allele frequencies in human.

$$\% \text{ depletion} = \frac{\text{MSR}_{\text{rare}} - \text{MSR}_{\text{comm}}}{\text{MSR}_{\text{rare}}}$$

The missense: synonymous ratios and the percentages of depletion were computed per species and are shown in Fig. 2b and Supplementary Table 2. In addition, for chimpanzee common variants (Fig. 1b), chimpanzee singleton variants (Fig. 1c), and mammal variants (Fig. 2a), we performed the χ^2 test of homogeneity on the 2×2 contingency table to test if the differences in missense: synonymous ratios between rare and common variants were significant.

Because sequencing was only performed on limited numbers of individuals from the great ape genome project, we used the human allele frequency spectrum from ExAC to estimate the fraction of sampled variants which were rare ($< 0.1\%$) or common ($> 0.1\%$) in the general chimpanzee population. We sampled a cohort of 24 humans based on the ExAC allele frequencies, and identified missense variants that were observed either once, or more than once, in this cohort. Variants that were observed more than once had a 99.8% chance of being common ($> 0.1\%$) in the general population, whereas variants that were observed only once in the cohort had a 69% chance of being common in the general population.

To verify that the observed depletion for missense variants in more distant mammals was not due to a confounding effect of genes that are better conserved, and hence more accurately aligned, we repeated the above analysis, restricting only to genes with $> 50\%$ average nucleotide identity in the multiple sequence alignment of 11 primates and 50 mammals compared with human (see Supplementary Table 3). This removed ~7% of human protein-coding genes from the analysis, without substantially affecting the results. Additionally, to ensure that our results were not affected by issues with variant calling, or domestication artifacts (since most of the species selected from dbSNP were domesticated), we repeated the analyses using fixed substitutions from pairs of closely-related species in lieu of intra-species polymorphisms (Fig. 2d, Supplementary Table 4, Supplementary Note, and Supplementary Data File 2).

ClinVar analysis of polymorphism data for human, primates, mammals, and other vertebrates

To examine the clinical impact of variants that are identical-by-state with other species, we downloaded the the ClinVar database (see URLs)[27], excluding variants those that had conflicting annotations of pathogenicity, or were only labeled as variants of uncertain significance. Following the filtering steps shown in Supplementary Table 9, there are a total of 24,853 missense variants in the pathogenic category and 17,775 missense variants in the benign category.

We counted the number of pathogenic and benign ClinVar variants that were identical-by-state with variation in humans, non-human primates, mammals and other vertebrates. For human, we simulated a cohort of 30 humans, sampled from ExAC allele frequencies. The numbers of benign and pathogenic variants for each species are shown in Supplementary Table 10.

Generation of benign and unlabeled variants for model training

We constructed a benign training dataset of largely common benign missense variants from human and non-human primates for machine learning. The dataset consisted of common human variants (> 0.1% allele frequency; 83,546 variants), and variants from chimpanzee, bonobo, gorilla, and orangutan, rhesus, and marmoset (301,690 unique primate variants). The number of benign training variants contributed by each source is shown in Supplementary Table 5.

We trained the deep learning network to discriminate between a set of labeled benign variants and an unlabeled set of variants that were matched to control for trinucleotide context, sequencing coverage, and alignability between the species and human. To obtain an unlabeled training dataset, all possible missense variants were generated from each base position of canonical coding regions by substituting the nucleotide at the position to the other three nucleotides. We excluded variants that were observed in the 123,136 exomes from ExAC, and variants in start or stop codons. In total, 68,258,623 unlabeled missense variants were generated. This was filtered to correct for regions of poor sequencing coverage, and regions where there was not a one-to-one alignment between human and primate genomes when selecting matched unlabeled variants for the primate variants. We obtained a consensus prediction by training eight models that use the same set of labeled benign variants and eight randomly sampled sets of unlabeled variants and taking the average of their predictions. We also set aside two randomly sampled two of 10,000 primate variants for validation and testing, which we withheld from training (Supplementary Data File 3). For each of these sets, we sampled 10,000 unlabeled variants that were matched by trinucleotide context, which we used to normalize the threshold of each classifier when comparing between different classification algorithms (Supplementary Data File 4).

We assessed the classification accuracy of two versions of the deep learning network, one trained with common human variants only, and one trained with the full benign labeled dataset including both common human variants and primate variants.

Architecture of the deep learning network

For each variant, the pathogenicity prediction network takes as input the 51-length amino acid sequence centered at the variant of interest, and the outputs of the secondary structure and solvent accessibility networks (Fig. 3a and Supplementary Fig. 4). To represent the variant, the network receives both the 51-length reference amino acid sequence ome and the alternative 51-length amino acid sequence with the missense variant substituted in at the central position. Three 51-length position frequency matrices (PFMs) are generated from multiple sequence alignments of 99 vertebrates, including one for 11 primates, one for 50 mammals excluding primates, and one for 38 vertebrates excluding primates and mammals.

The secondary structure deep learning network predicts 3-state secondary structure at each amino acid position: alpha helix (H), beta sheet (B), and coils (C) (Supplementary Table 11). The solvent accessibility network predicts 3-state solvent accessibility at each amino acid position: buried (B), intermediate (I), and exposed (E) (Supplementary Table 12). Both networks only take the flanking amino acid sequence as their inputs, and were trained using labels from known non-redundant crystal structures in the Protein DataBank (Supplementary Note and Supplementary Table 13). For the input to the pre-trained 3-state secondary structure and 3-state solvent accessibility networks, we used a single PFM matrix generated from the multiple sequence alignments for all 99 vertebrates, also with length 51 and depth 20. After pre-training the networks on known crystal structures from the Protein DataBank, the final two layers for the secondary structure and solvent models were removed and the output of the network was directly connected to the input of the pathogenicity model. The best testing accuracy achieved for the 3-state secondary structure prediction model is 79.86 % (Supplementary Table 14). There was no substantial difference when comparing the predictions of the neural network when using DSSP-annotated[72,73] structure labels for the approximately ~4000 human proteins that had crystal structures, versus using predicted structure labels only (Supplementary Table 15).

Both our deep learning network for pathogenicity prediction (PrimateAI) and deep learning networks for predicting secondary structure and solvent accessibility adopted the architecture of residual blocks[49,74]. The detailed architecture for PrimateAI is described in Supplementary Fig. 4 and Supplementary Table 16. The detailed architecture for the networks for predicting secondary structure and solvent accessibility is described in Supplementary Fig. 5 and Supplementary Tables 11 and 12.

Benchmarking of classifier performance on a withheld test set of 10,000 primate variants

We used the 10,000 withheld primate variants in the test dataset to benchmark the deep learning network as well as the other 20 previously published classifiers[32–39,41,42,44,46,47,75–79], for which we obtained prediction scores from dbNSFP[80] (see URLs). The performance for each of the classifiers on the 10,000 withheld primate variant test set is provided in Supplementary Fig. 9a. Because the different classifiers had widely varying score distributions, we used 10,000 randomly selected unlabeled variants that were matched to the test set by trinucleotide context to identify the 50th percentile threshold for each classifier. We benchmarked each classifier on the fraction of variants in the 10,000 withheld primate variant test set that were classified as benign at the 50th percentile threshold for that classifier, to ensure fair comparison between the methods.

For each of the classifiers, the fraction of withheld primate test variants predicted as benign using the 50th percentile threshold is shown (Supplementary Fig. 9a and Supplementary Table 17). We also show that the performance of PrimateAI is robust with respect to the number of aligned species at the variant position, and generally performs well as long as sufficient conservation information from mammals is available, which is true for most protein-coding sequence (Supplementary Fig. 14).

Analysis of *de novo* variants from the DDD study

We obtained published *de novo* variants from the Deciphering Developmental Disorders (DDD) study[64,65], and *de novo* variants from the healthy sibling controls in the Simons Simplex Collection (SSC) autism study[66]. The DDD study provides a confidence level for *de novo* variants, and we excluded variants from the DDD dataset with a threshold of < 0.1 as potential false positives due to variant calling errors. In total, we had 3,512 missense *de novo* variants from DDD affected individuals and 1,208 missense *de novo* variants from healthy controls. The canonical transcript annotations used by UCSC for the 99-vertebrate multiple-sequence alignment differed slightly from the transcript annotations used by DDD, resulting in a small difference in the total counts of missense variants. We evaluated the classification methods on their ability to discriminate between *de novo* missense variants in the DDD affected individuals, versus *de novo* missense variants in unaffected sibling controls from the autism studies. For each classifier, we reported the p-value from the Wilcoxon rank-sum test of the difference between the prediction scores for the two distributions (Supplementary Fig. 9b, c and Supplementary Table 17).

To measure the accuracy of various classifiers at distinguishing benign and pathogenic variation within the same disease gene, we repeated the analysis on only a set of 605 genes that were enriched for *de novo* protein-truncating variation in the DDD cohort (p<0.05, Poisson exact test) (Supplementary Table 18). Within these 605 genes, we estimated that 2/3 of the *de novo* variants in the DDD dataset were pathogenic and 1/3 were benign, based on the 3:1 enrichment of *de novo* missense mutations over expectation. We assumed minimal incomplete penetrance and that the *de novo* missense mutations in the healthy controls were benign. To estimate the accuracy of each classifier to each *de novo* mutations in the DDD and healthy control datasets, we identified the threshold that produced the same number of benign or pathogenic predictions as the empirical proportions observed in these datasets, and used this threshold as a binary cutoff to estimate the accuracy of each classifier at distinguishing *de novo* mutations in cases versus controls.

To construct a receiver operator characteristics curve, we treated pathogenic classification of *de novo* DDD variants as true positive calls, and treated classification of *de novo* variants in healthy controls as pathogenic as being false positive calls. Because the DDD dataset is contains 1/3 benign *de novo* variants, the area under the curve (AUC) for a theoretically perfect classifier is less than one[81]. Hence, a classifier with perfect separation of benign and pathogenic variants would classify 67% of *de novo* variants in the DDD patients as true positives, 33% of *de novo* variants in the DDD patients as false negatives, and 100% of *de novo* variants in controls as true negatives, yielding a maximum possible AUC of 0.837 (Supplementary Fig. 10, Supplementary Table 19, and Supplementary Note).

Novel candidate gene discovery

We tested enrichment of *de novo* mutations in genes by comparing the observed number of *de novo* mutations to the number expected under a null mutation model[14]. We repeated the enrichment analysis performed in the DDD study, and report genes that are newly genome-wide significant when only counting *de novo* missense mutations with a PrimateAI score of > 0.803. We adjusted the genome-wide expectation for *de novo* damaging missense variation

by the fraction of missense variants that meet the PrimateAI threshold of > 0.803 (roughly ~1/5th of all possible missense mutations genome-wide). As per the DDD study, each gene required four tests, one testing protein truncating enrichment, and one testing enrichment of protein-altering *de novo* mutations, both tested for just the DDD cohort[65], and for a larger meta-analysis of neurodevelopmental trio sequencing cohorts[62,63,66,82–89]. The enrichment of protein-altering *de novo* mutations was combined by Fisher's method with a test of the clustering of missense *de novo* mutations within the coding sequence (Supplementary Tables 20, 21). The p-value for each gene was taken from the minimum of the four tests, and genome-wide significance was determined as $P < 6.757 \times 10^{-7}$ (α=0.05, 18,500 genes with four tests).

ClinVar classification accuracy

Since most of the existing classifiers are either trained directly or indirectly on ClinVar content, such as using prediction scores from classifiers that are trained on ClinVar, we limited analysis of the ClinVar dataset to only use ClinVar variants that were added since 2017. There was substantial overlap among the recent ClinVar variants and other databases, and hence we further filtered to remove found at common allele frequencies (> 0.1%) in ExAC, or present in HGMD, LSDB, or Uniprot[90–92]. After excluding variants annotated only as uncertain significance and those with conflicting annotations, we were left with 177 missense variants with benign annotation and 969 missense variants with pathogenic annotation. We scored these ClinVar variants using both the deep learning network and ther other classification methods. For each classifier, we identified the threshold that produced the same number of benign or pathogenic predictions as the empirical proportions observed in these datasets, and used this threshold as a binary cutoff to estimate the accuracy of each classifier (Supplementary Fig. 12).

Impact of increasing training data size and using different sources of training data

To evaluate the impact of training data size on the performance of the deep learning network, we randomly sampled a subset of variants from the labeled benign training set of 385,236 primate and common human variants, and kept the underlying deep learning network architecture the same. To show that variants from each individual primate species contributes to classification accuracy whereas variants from each individual mammal species lower classification accuracy, we trained deep learning networks using a training dataset consisting of 83,546 human variants plus a constant number of randomly selected variants for each species, again keeping the underlying network architecture the same. The constant number of variants we added to the training set (23,380) is the total number of variants available in the species with the lowest number of missense variants, i.e. bonobo. We repeated the training procedures five times to get the median performance of each classifier.

Saturation of all possible human missense mutations with increasing number of primate populations sequenced

We investigated the expected saturation of all ~70M possible human missense mutations by common variants present in the 504 extant primate species, by simulating variants based on the trinucleotide context of human common missense variants (> 0.1% allele frequency) observed in ExAC. For each primate species, we simulated 4 times the number of common

missense variants observed in human (~83,500 missense variants with allele frequency > 0.1%), because humans have roughly half the number of variants per individual as other primate species[13], and about ~50% of human missense variants have been filtered out by purifying selection at > 0.1% allele frequency (Fig. 1a and Supplementary Note).

To model the fraction of human common missense variants (> 0.1% allele frequency) discovered with increasing size of human cohorts surveyed (Supplementary Fig. 13), we sampled genotypes according to ExAC allele frequencies and report the fraction of common variants that were observed at least once in these simulated cohorts.

URLs

Data downloaded from UCSC genome browser: http://hgdownload.soe.ucsc.edu/goldenPath/hg19/multiz100way/alignments/knownCanonical.exonNuc.fa.gz, http://hgdownload.soe.ucsc.edu/goldenPath/hg19/multiz100way/hg19.100way.commonNames.nh; ExAC/gnomAD data: http://gnomad.broadinstitute.org/; ClinVar database released on 02-Nov-2017: ftp://ftp.ncbi.nlm.nih.gov/pub/clinvar/clinvar_20171029.vcf.gz; dbNSFP: https://sites.google.com/site/jpopgen/dbNSFP; PrimateAI scores of 70M variants: https://basespace.illumina.com/s/cPgCSmecvhb4; Life Sciences Reporting Summary: https://www.nature.com/authors/policies/ReportingSummary.pdf

Data and code availability

Prediction scores for all 70M human missense variants on the hg19/GRCh37 genome build with the human+primate deep learning network (PrimateAI) are publicly hosted (see URLs). For practical application of PrimateAI scores, we recommend a threshold of > 0.8 for likely pathogenic classification, < 0.6 for likely benign, and 0.6–0.8 as intermediate, based on the enrichment of *de novo* variants in cases compared to controls (Fig. 3d).

To reduce problems with circularity that have become a concern for the field, the authors explicitly request that the prediction scores from the method not be incorporated as a component of other classifiers, and instead ask that interested parties employ the provided source code and data to directly train and improve upon their own deep learning models. Similarly, the authors request that the 10,000 withheld primate variants (Supplementary Data File 3) not be used for training future classifiers, in order to provide the community with an independent truth dataset for benchmarking.

Supplementary Material

Refer to Web version on PubMed Central for supplementary material.

Acknowledgments

References

1. MacArthur DG, et al. Guidelines for investigating causality of sequence variants in human disease. Nature. 2014; 508:469–476. DOI: 10.1038/nature13127 [PubMed: 24759409]

2. Rehm HL, Berg JS, Brooks LD, Bustamante CD, Evans JP, Landrum MJ, Ledbetter DH, Maglott DR, Martin CL, Nussbaum RL, Plon SE, Ramos EM, Sherry ST, Watson MS. ClinGen--the Clinical Genome Resource. N Engl J Med. 2015; 372:2235–2242. [PubMed: 26014595]

3. Bamshad MJ, Ng SB, Bigham AW, Tabor HK, Emond MJ, Nickerson DA, Shendure J. Exome sequencing as a tool for Mendelian disease gene discovery. Nat Rev Genet. 2011; 12:745–755. [PubMed: 21946919]

4. Rehm HL. Evolving health care through personal genomics. Nature Reviews Genetics. 2017; 18:259–267.

5. Richards S, et al. Standards and guidelines for the interpretation of sequence variants: a joint consensus recommendation of the American College of Medical Genetics and Genomics and the Association for Molecular Pathology. Genet Med. 2015; 17:405–424. DOI: 10.1038/gim.2015.30 [PubMed: 25741868]

6. Lek M, et al. Analysis of protein-coding genetic variation in 60,706 humans. Nature. 2016; 536:285–291. DOI: 10.1038/nature19057 [PubMed: 27535533]

7. Mallick S, et al. The Simons Genome Diversity Project: 300 genomes from 142 diverse populations. Nature. 2016; 538:201–206. DOI: 10.1038/nature18964 [PubMed: 27654912]

8. Genomes Project Consortium et al. A global reference for human genetic variation. Nature. 2015; 526:68–74. DOI: 10.1038/nature15393 [PubMed: 26432245]

9. Liu X, Jian X, Boerwinkle E. dbNSFP: A lightweight database of human nonsynonymous SNPs and their functional predictions. Human Mutation. 2011; 32:894–899. [PubMed: 21520341]

10. Chimpanzee Sequencing Analysis Consortium. Initial sequence of the chimpanzee genome and comparison with the human genome. Nature. 2005; 437:69–87. DOI: 10.1038/nature04072 [PubMed: 16136131]

11. Takahata N. Allelic genealogy and human evolution. Mol Biol Evol. 1993; 10:2–22. [PubMed: 8450756]

12. Asthana S, Schmidt S, Sunyaev S. A limited role for balancing selection. Trends Genet. 2005; 21:30–32. DOI: 10.1016/j.tig.2004.11.001 [PubMed: 15680511]

13. Leffler EM, Gao Z, Pfeifer S, Ségurel L, Auton A, Venn O, Bowden R, Bontrop R, Wall JD, Sella G, Donnelly P. Multiple instances of ancient balancing selection shared between humans and chimpanzees. Science. 2013; 339:1578–1582. [PubMed: 23413192]

14. Samocha KE, et al. A framework for the interpretation of *de novo* mutation in human disease. Nat Genet. 2014; 46:944–950. DOI: 10.1038/ng.3050 [PubMed: 25086666]

15. Ohta T. Slightly deleterious mutant substitutions in evolution. Nature. 1973; 246:96–98. [PubMed: 4585855]

16. Reich DE, Lander ES. On the allelic spectrum of human disease. Trends Genet. 2001; 17:502–510. [PubMed: 11525833]

17. Whiffin N, Minikel E, Walsh R, O'Donnell-Luria AH, Karczewski K, Ing AY, Barton PJ, Funke B, Cook SA, MacArthur D, Ware JS. Using high-resolution variant frequencies to empower clinical genome interpretation. Genetics in Medicine. 2017; 19:1151–1158. [PubMed: 28518168]

18. Prado-Martinez J, et al. Great ape genome diversity and population history. Nature. 2013; 499:471–475. [PubMed: 23823723]

19. Klein J, Satta Y, O'HUigin C, Takahata N. The molecular descent of the major histocompatibility complex. Annu Rev Immunol. 1993; 11:269–295. DOI: 10.1146/annurev.iy.11.040193.001413 [PubMed: 8476562]

20. Kimura M. The neutral theory of molecular evolution. Cambridge University Press; 1983.

21. de Manuel M, et al. Chimpanzee genomic diversity reveals ancient admixture with bonobos. Science. 2016; 354:477–481. DOI: 10.1126/science.aag2602 [PubMed: 27789843]

22. Locke DP, et al. Comparative and demographic analysis of orang-utan genomes. Nature. 2011; 469:529–533. [PubMed: 21270892]

23. Rhesus Macaque Genome Sequencing Analysis Consortium et al. Evolutionary and biomedical insights from the rhesus macaque genome. Science. 2007; 316:222–234. DOI: 10.1126/science.1139247 [PubMed: 17431167]

24. Worley KC, Warren WC, Rogers J, Locke D, Muzny DM, Mardis ER, Weinstock GM, Tardif SD, Aagaard KM, Archidiacono N, Rayan NA. The common marmoset genome provides insight into primate biology and evolution. Nature Genetics. 2014; 46:850–857. [PubMed: 25038751]

25. Sherry ST, et al. dbSNP: the NCBI database of genetic variation. Nucleic Acids Res. 2001; 29:308–311. [PubMed: 11125122]

26. Schrago CG, Russo CA. Timing the origin of New World monkeys. Mol Biol Evol. 2003; 20:1620–1625. DOI: 10.1093/molbev/msg172 [PubMed: 12832653]

27. Landrum MJ, et al. ClinVar: public archive of interpretations of clinically relevant variants. Nucleic Acids Res. 2016; 44:D862–868. DOI: 10.1093/nar/gkv1222 [PubMed: 26582918]

28. Brandon EP, Idzerda RL, McKnight GS. Targeting the mouse genome: a compendium of knockouts (Part II). Curr Biol. 1995; 5:758–765. [PubMed: 7583122]

29. Lieschke JG, Currie PD. Animal models of human disease: zebrafish swim into view. Nature Reviews Genetics. 2007; 8:353–367.

30. Sittig LJ, Carbonetto P, Engel KA, Krauss KS, Barrios-Camacho CM, Palmer AA. Genetic background limits generalizability of genotype-phenotype relationships. Neuron. 2016; 91:1253–1259. [PubMed: 27618673]

31. Bazykin GA, et al. Extensive parallelism in protein evolution. Biol Direct. 2007; 2:20. [PubMed: 17705846]

32. Ng PC, Henikoff S. Predicting deleterious amino acid substitutions. Genome Res. 2001; 11:863–874. DOI: 10.1101/gr.176601 [PubMed: 11337480]

33. Adzhubei IA, et al. A method and server for predicting damaging missense mutations. Nat Methods. 2010; 7:248–249. DOI: 10.1038/nmeth0410-248 [PubMed: 20354512]

34. Chun S, Fay JC. Identification of deleterious mutations within three human genomes. Genome research. 2009; 19:1553–1561. [PubMed: 19602639]

35. Schwarz JM, Rödelsperger C, Schuelke M, Seelow D. MutationTaster evaluates disease-causing potential of sequence alterations. Nat Methods. 2010; 7:575–576. [PubMed: 20676075]

36. Reva B, Antipin Y, Sander C. Predicting the functional impact of protein mutations: application to cancer genomics. Nucleic Acids Res. 2011; 39:e118. [PubMed: 21727090]

37. Dong C, et al. Comparison and integration of deleteriousness prediction methods for nonsynonymous SNVs in whole exome sequencing studies. Hum Mol Genet. 2015; 24:2125–2137. DOI: 10.1093/hmg/ddu733 [PubMed: 25552646]

38. Carter H, Douville C, Stenson PD, Cooper DN, Karchin R. Identifying Mendelian disease genes with the variant effect scoring tool. BMC Genomics. 2013; 14(Suppl 3):S3.

39. Choi Y, Sims GE, Murphy S, Miller JR, Chan AP. Predicting the functional effect of amino acid substitutions and indels. PLoS One. 2012; 7:e46688. [PubMed: 23056405]

40. Gulko B, Hubisz MJ, Gronau I, Siepel A. A method for calculating probabilities of fitness consequences for point mutations across the human genome. Nat Genet. 2015; 47:276–283. DOI: 10.1038/ng.3196 [PubMed: 25599402]

41. Shihab HA, et al. An integrative approach to predicting the functional effects of non-coding and coding sequence variation. Bioinformatics. 2015; 31:1536–1543. DOI: 10.1093/bioinformatics/btv009 [PubMed: 25583119]

42. Quang D, Chen Y, Xie X. DANN: a deep learning approach for annotating the pathogenicity of genetic variants. Bioinformatics. 2015; 31:761–763. DOI: 10.1093/bioinformatics/btu703 [PubMed: 25338716]

43. Bell CJ, Dinwiddie DL, Miller NA, Hateley SL, Ganusova EE, Midge J, Langley RJ, Zhang L, Lee CL, Schilkey RD, Woodward JE, Peckham HE, Schroth GP, Kim RW, Kingsmore SF. Comprehensive carrier testing for severe childhood recessive diseases by next generation sequencing. Sci Transl Med. 2011; 3:65ra64.

44. Kircher M, Witten DM, Jain P, O'Roak BJ, Cooper GM, Shendure J. A general framework for estimating the relative pathogenicity of human genetic variants. Nat Genet. 2014; 46:310–315. [PubMed: 24487276]

45. Smedley D, et al. A Whole-Genome Analysis Framework for Effective Identification of Pathogenic Regulatory Variants in Mendelian Disease. Am J Hum Genet. 2016; 99:595–606. DOI: 10.1016/j.ajhg.2016.07.005 [PubMed: 27569544]

46. Ioannidis NM, et al. REVEL: an ensemble method for predicting the pathogenicity of rare missense variants. Am J Hum Genet. 2016; 99:877–885. DOI: 10.1016/j.ajhg.2016.08.016 [PubMed: 27666373]

47. Jagadeesh KA, Wenger AM, Berger MJ, Guturu H, Stenson PD, Cooper DN, Bernstein JA, Bejerano G. M-CAP eliminates a majority of variants of uncertain significance in clinical exomes at high sensitivity. Nature genetics. 2016; 48:1581–1586. [PubMed: 27776117]

48. Grimm DG. The evaluation of tools used to predict the impact of missense variants is hindered by two types of circularity. Human mutation. 2015; 36:513–523. [PubMed: 25684150]

49. He K, Zhang X, Ren S, Sun J. Proceedings of the IEEE conference on computer vision and pattern recognition; 770–778.

50. Heffernan R, et al. Improving prediction of secondary structure, local backbone angles, and solvent accessible surface area of proteins by iterative deep learning. Sci Rep. 2015; 5:11476. [PubMed: 26098304]

51. Wang S, Peng J, Ma J, Xu J. Protein secondary structure prediction using deep convolutional neural fields. Scientific reports. 2016; 6:18962–18962. [PubMed: 26752681]

52. Harpak A, Bhaskar A, Pritchard JK. Mutation Rate Variation is a Primary Determinant of the Distribution of Allele Frequencies in Humans. PLoS Genetics. 2016; 12

53. Payandeh J, Scheuer T, Zheng N, Catterall WA. The crystal structure of a voltage-gated sodium channel. Nature. 2011; 475:353–358. [PubMed: 21743477]

54. Shen H, et al. Structure of a eukaryotic voltage-gated sodium channel at near-atomic resolution. Science. 2017; 355:eaal4326. [PubMed: 28183995]

55. Nakamura K, et al. Clinical spectrum of SCN2A mutations expanding to Ohtahara syndrome. Neurology. 2013; 81:992–998. DOI: 10.1212/WNL.0b013e3182a43e57 [PubMed: 23935176]

56. Henikoff S, Henikoff JG. Amino acid substitution matrices from protein blocks. Proc Natl Acad Sci U S A. 1992; 89:10915–10919. [PubMed: 1438297]

57. Li WH, Wu CI, Luo CC. Nonrandomness of point mutation as reflected in nucleotide substitutions in pseudogenes and its evolutionary implications. Journal of Molecular Evolution. 1984; 21:58–71. [PubMed: 6442359]

58. Grantham R. Amino acid difference formula to help explain protein evolution. Science. 1974; 185:862–864. [PubMed: 4843792]

59. LeCun Y, Bottou L, Bengio Y, Haffner P. Proceedings of the IEEE. :2278–2324.

60. Vissers LE, Gilissen C, Veltman JA. Genetic studies in intellectual disability and related disorders. Nat Rev Genet. 2016; 17:9–18. DOI: 10.1038/nrg3999 [PubMed: 26503795]

61. Neale BM, et al. Patterns and rates of exonic *de novo* mutations in autism spectrum disorders. Nature. 2012; 485:242–245. DOI: 10.1038/nature11011 [PubMed: 22495311]

62. Sanders SJ, et al. De novo mutations revealed by whole-exome sequencing are strongly associated with autism. Nature. 2012; 485:237–241. DOI: 10.1038/nature10945 [PubMed: 22495306]

63. De Rubeis S, et al. Synaptic, transcriptional and chromatin genes disrupted in autism. Nature. 2014; 515:209–215. DOI: 10.1038/nature13772 [PubMed: 25363760]

64. Deciphering Developmental Disorders Study. Large-scale discovery of novel genetic causes of developmental disorders. Nature. 2015; 519:223–228. DOI: 10.1038/nature14135 [PubMed: 25533962]

65. Deciphering Developmental Disorders Study. Prevalence and architecture of *de novo* mutations in developmental disorders. Nature. 2017; 542:433–438. DOI: 10.1038/nature21062 [PubMed: 28135719]

66. Iossifov I, et al. The contribution of *de novo* coding mutations to autism spectrum disorder. Nature. 2014; 515:216–221. DOI: 10.1038/nature13908 [PubMed: 25363768]

67. Zhu X, Need AC, Petrovski S, Goldstein DB. One gene, many neuropsychiatric disorders: lessons from Mendelian diseases. Nat Neurosci. 2014; 17:773–781. DOI: 10.1038/nn.3713 [PubMed: 24866043]

68. Leffler EM, Bullaughey K, Matute DR, Meyer WK, Ségurel L, Venkat A, Andolfatto P, Przeworski M. Revisiting an old riddle: what determines genetic diversity levels within species? PLoS biology. 2012; 10:e1001388. [PubMed: 22984349]

69. Estrada A, et al. Impending extinction crisis of the world's primates: Why primates matter. Science advances. 2017; 3:e1600946. [PubMed: 28116351]

70. Kent WJ, Sugnet CW, Furey TS, Roskin KM, Pringle TH, Zahler AM, Haussler D. The human genome browser at UCSC. Genome Res. 2002; 12:996–1006. [PubMed: 12045153]

71. Tyner C, et al. The UCSC Genome Browser database: 2017 update. Nucleic Acids Res. 2017; 45:D626–D634. DOI: 10.1093/nar/gkw1134 [PubMed: 27899642]

72. Kabsch W, Sander C. Dictionary of protein secondary structure: pattern recognition of hydrogen-bonded and geometrical features. Biopolymers. 1983; 22:2577–2637. DOI: 10.1002/bip. 360221211 [PubMed: 6667333]

73. Joosten RP, et al. A series of PDB related databases for everyday needs. Nucleic Acids Res. 2011; 39:D411–419. DOI: 10.1093/nar/gkq1105 [PubMed: 21071423]

74. He K, Zhang X, Ren S, Sun J. European Conference on Computer Vision. Springer; 630–645.

75. Ionita-Laza I, McCallum K, Xu B, Buxbaum JD. A spectral approach integrating functional genomic annotations for coding and noncoding variants. Nat Genet. 2016; 48:214–220. DOI: 10.1038/ng.3477 [PubMed: 26727659]

76. Li B, et al. Automated inference of molecular mechanisms of disease from amino acid substitutions. Bioinformatics. 2009; 25:2744–2750. DOI: 10.1093/bioinformatics/btp528 [PubMed: 19734154]

77. Lu Q, et al. A statistical framework to predict functional non-coding regions in the human genome through integrated analysis of annotation data. Sci Rep. 2015; 5:10576. [PubMed: 26015273]

78. Shihab HA, et al. Predicting the functional, molecular, and phenotypic consequences of amino acid substitutions using hidden Markov models. Hum Mutat. 2013; 34:57–65. DOI: 10.1002/humu. 22225 [PubMed: 23033316]

79. Davydov EV, et al. Identifying a high fraction of the human genome to be under selective constraint using GERP++ PLoS Comput Biol. 2010; 6:e1001025. [PubMed: 21152010]

80. Liu X, Wu C, Li C, Boerwinkle E. dbNSFP v3.0: A One-Stop Database of Functional Predictions and Annotations for Human Nonsynonymous and Splice-Site SNVs. Hum Mutat. 2016; 37:235–241. DOI: 10.1002/humu.22932 [PubMed: 26555599]

81. Jain S, White M, Radivojac P. Proceedings of the Thirty-First AAAI Conference on Artificial Intelligence; 2066–2072.

82. de Ligt J, et al. Diagnostic exome sequencing in persons with severe intellectual disability. N Engl J Med. 2012; 367:1921–1929. DOI: 10.1056/NEJMoa1206524 [PubMed: 23033978]

83. Iossifov I, et al. De novo gene disruptions in children on the autistic spectrum. Neuron. 2012; 74:285–299. DOI: 10.1016/j.neuron.2012.04.009 [PubMed: 22542183]

84. O'Roak BJ, et al. Sporadic autism exomes reveal a highly interconnected protein network of *de novo* mutations. Nature. 2012; 485:246–250. DOI: 10.1038/nature10989 [PubMed: 22495309]

85. Rauch A, et al. Range of genetic mutations associated with severe non-syndromic sporadic intellectual disability: an exome sequencing study. Lancet. 2012; 380:1674–1682. DOI: 10.1016/ S0140-6736(12)61480-9 [PubMed: 23020937]

86. Epi KC, et al. De novo mutations in epileptic encephalopathies. Nature. 2013; 501:217–221. DOI: 10.1038/nature12439 [PubMed: 23934111]

87. Euro E-RESC, Epilepsy Phenome/Genome P, Epi KC. De novo mutations in synaptic transmission genes including DNM1 cause epileptic encephalopathies. Am J Hum Genet. 2014; 95:360–370. DOI: 10.1016/j.ajhg.2014.08.013 [PubMed: 25262651]

88. Gilissen C, et al. Genome sequencing identifies major causes of severe intellectual disability. Nature. 2014; 511:344–347. DOI: 10.1038/nature13394 [PubMed: 24896178]

89. Lelieveld SH, et al. Meta-analysis of 2,104 trios provides support for 10 new genes for intellectual disability. Nat Neurosci. 2016; 19:1194–1196. DOI: 10.1038/nn.4352 [PubMed: 27479843]

90. Famiglietti ML, et al. Genetic variations and diseases in UniProtKB/Swiss-Prot: the ins and outs of expert manual curation. Hum Mutat. 2014; 35:927–935. DOI: 10.1002/humu.22594 [PubMed: 24848695]

91. Horaitis O, Talbot CC Jr, Phommarinh M, Phillips KM, Cotton RG. A database of locus-specific databases. Nat Genet. 2007; 39:425. [PubMed: 17392794]

92. Stenson PD, et al. The Human Gene Mutation Database: building a comprehensive mutation repository for clinical and molecular genetics, diagnostic testing and personalized genomic medicine. Hum Genet. 2014; 133:1–9. DOI: 10.1007/s00439-013-1358-4 [PubMed: 24077912]
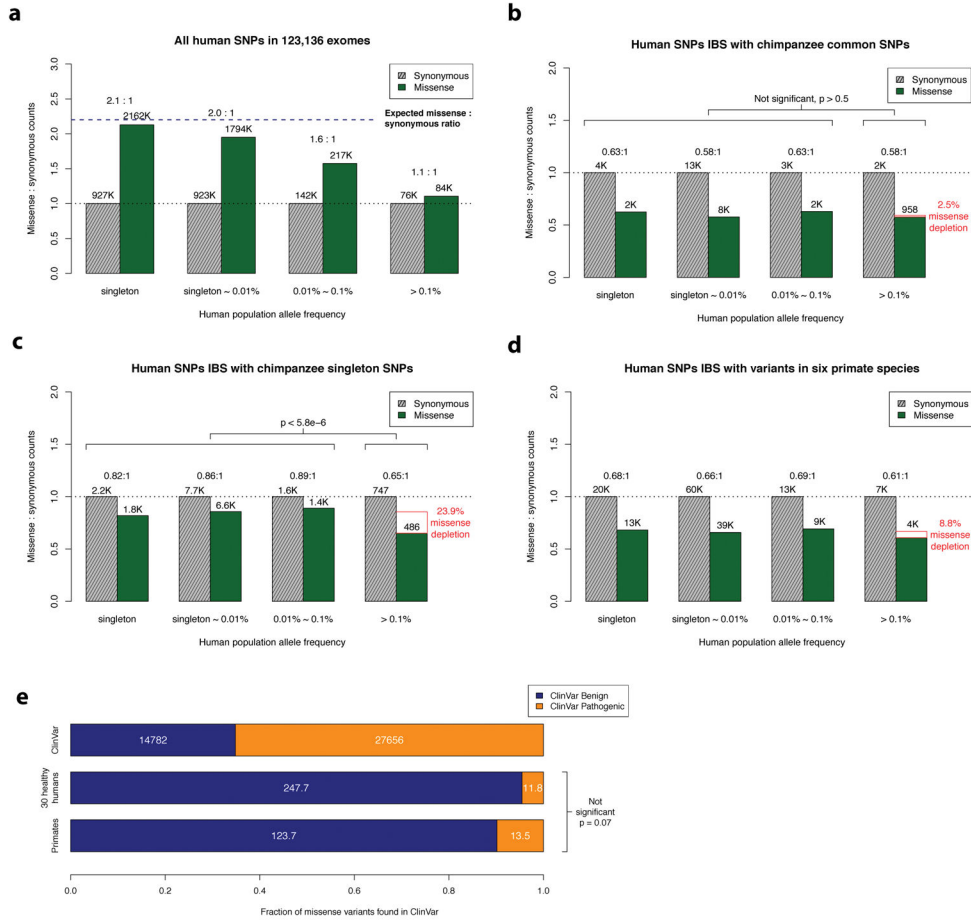
Figure 1. Missense: synonymous ratios across the human allele frequency spectrum
a, All missense and synonymous variants observed in 123,136 humans from the ExAC/
gnomAD database were divided into 4 categories by allele frequency. Shaded grey bars
represent counts of synonymous variants in each category; dark green bars represent
missense variants. The height of each bar is scaled to the number of synonymous variants in
each allele frequency category and the missense: synonymous counts and ratios are
displayed after adjusting for mutation rate. **b**, **c**, Allele frequency spectrum for human
missense and synonymous variants that are identical-by-state (IBS) with (**b**) chimpanzee
common and (**c**) chimpanzee singleton variants. The depletion of chimpanzee missense
variants at common human allele frequencies (>0.1%) compared to rare human allele
frequencies (< 0.1%) is indicated by the red box, along with accompanying χ^2 test p-values.
d, As in (**b**) and (**c**), but using human variants that are observed in at least one of the non-
human primate species. **e**, Counts of benign and pathogenic missense variants in the overall
ClinVar database (top row), compared to ClinVar variants in a cohort of 30 humans sampled
from ExAC/gnomAD allele frequencies (middle row), compared to variants observed in
primates (bottom row). Conflicting benign and pathogenic assertions and variants annotated
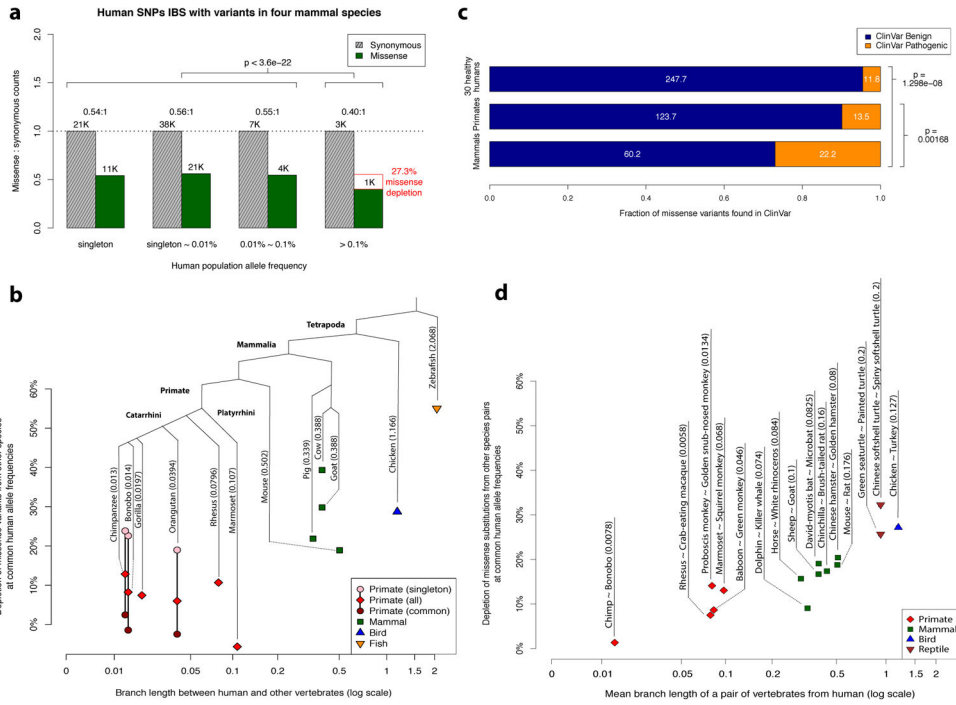only with uncertain significance were excluded.

Figure 2. Purifying selection on missense variants identical-by-state with other species
a, Allele frequency spectrum for human missense and synonymous variants that are identical-by-state with variants present in four non-primate mammalian species (mouse, pig, goat, cow). The depletion of missense variants at common human allele frequencies (>0.1%) is indicated by the red box, along with the accompanying χ^2 test p-value. **b**, Scatter plot showing the depletion of missense variants observed in other species at common human allele frequencies (>0.1%) versus the species' evolutionary distance from human, expressed in units of branch length (mean number of substitutions per nucleotide position). The total branch length between that species number appearing in parentheses beside each species' name indicates the total branch length between that species and human. Depletion values for singleton and common variants are shown for species where variant frequencies were available, with the exception of gorilla, which contained related individuals. **c**, Counts of benign and pathogenic missense variants in a cohort of 30 humans sampled from ExAC/ gnomAD allele frequencies (top row), compared to variants observed in primates (middle row), and compared to variants observed in mouse, pig, goat, and cow (bottom row). Conflicting benign and pathogenic assertions and variants annotated only with uncertain significance were excluded. **d**, Scatter plot showing the depletion of fixed missense substitutions observed in pairs of closely related species at common human allele frequencies (>0.1%) versus the species'evolutionary distance from human (expressed in units of mean branch length).
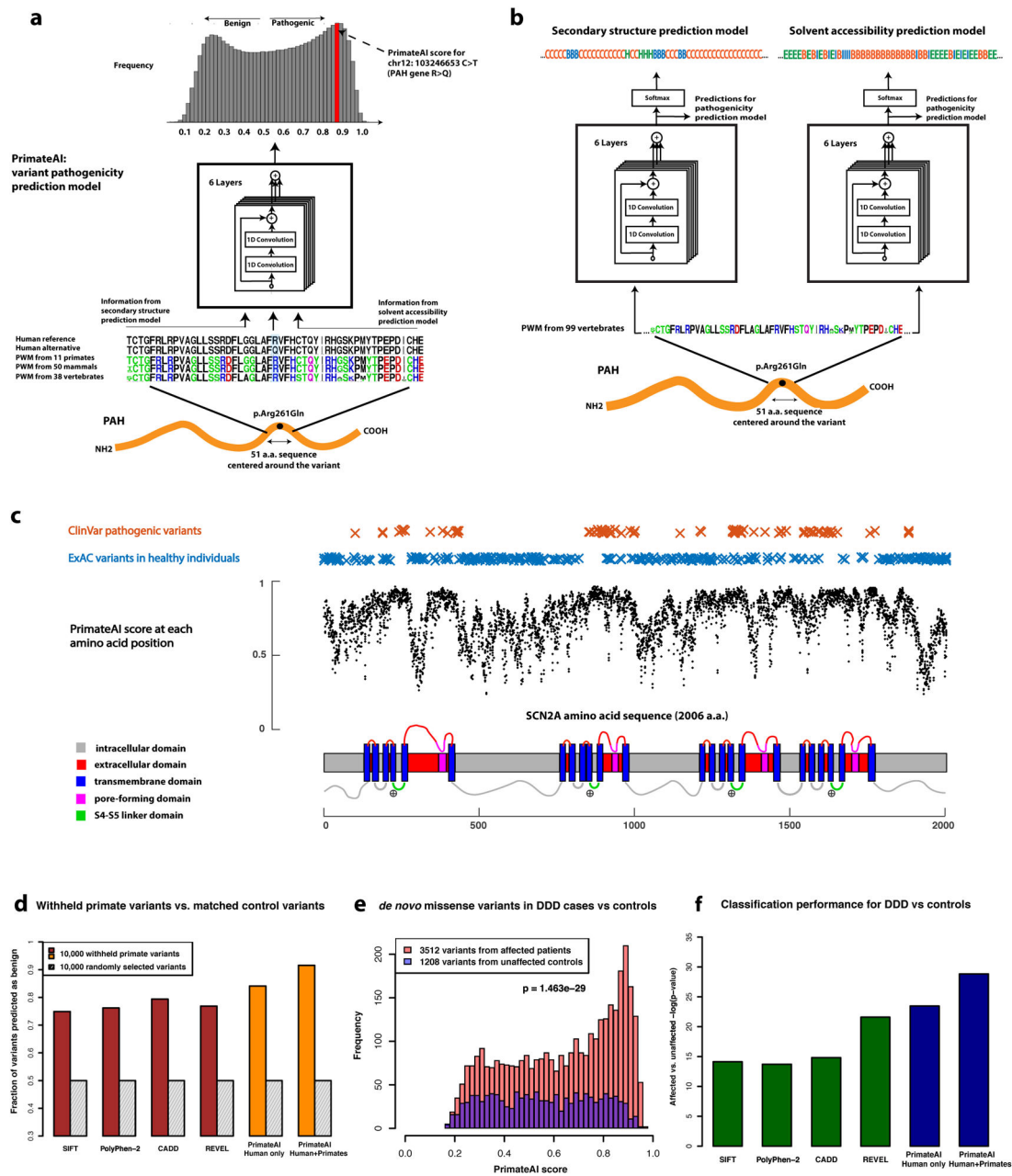
Figure 3. Deep learning network for classification of missense variants
a, Architecture of the deep learning network for pathogenicity prediction, PrimateAI. Predicted pathogenicity is on a scale from 0 (benign) to 1 (pathogenic). The network takes as input the human amino acid (AA) reference and alternate sequence (51 AAs) centered at the variant, the position weight matrix (PWM) conservation profiles calculated from 99 vertebrate species, and **b**, the outputs of secondary structure and solvent accessibility prediction deep learning networks, which predict three-state protein secondary structure (helix—H, beta sheet—B, and coil—C) and three-state solvent accessibility (buried—B, intermediate—I, and exposed—E). **c**, Predicted pathogenicity score at each amino acid position in the SCN2A gene, annotated for key functional domains. Plotted along the gene is

the average PrimateAI score for missense substitutions at each amino acid position. **d**, Comparison of classifiers at predicting benign consequence for a test set of 10,000 common primate variants that were withheld from training. The y-axis represents the percentage of primate variants correctly classified as benign, after normalizing the threshold of each classifier to its 50th percentile score on a set of 10,000 random variants that were matched for mutational rate. **e**, Distributions of PrimateAI prediction scores for *de novo* missense variants occurring in DDD patients compared to unaffected siblings, with corresponding Wilcoxon rank-sum p-value. **f**, Comparison of classifiers at separating *de novo* missense variants in DDD cases versus controls. Wilcoxon rank-sum test p-values are shown for each classifier.
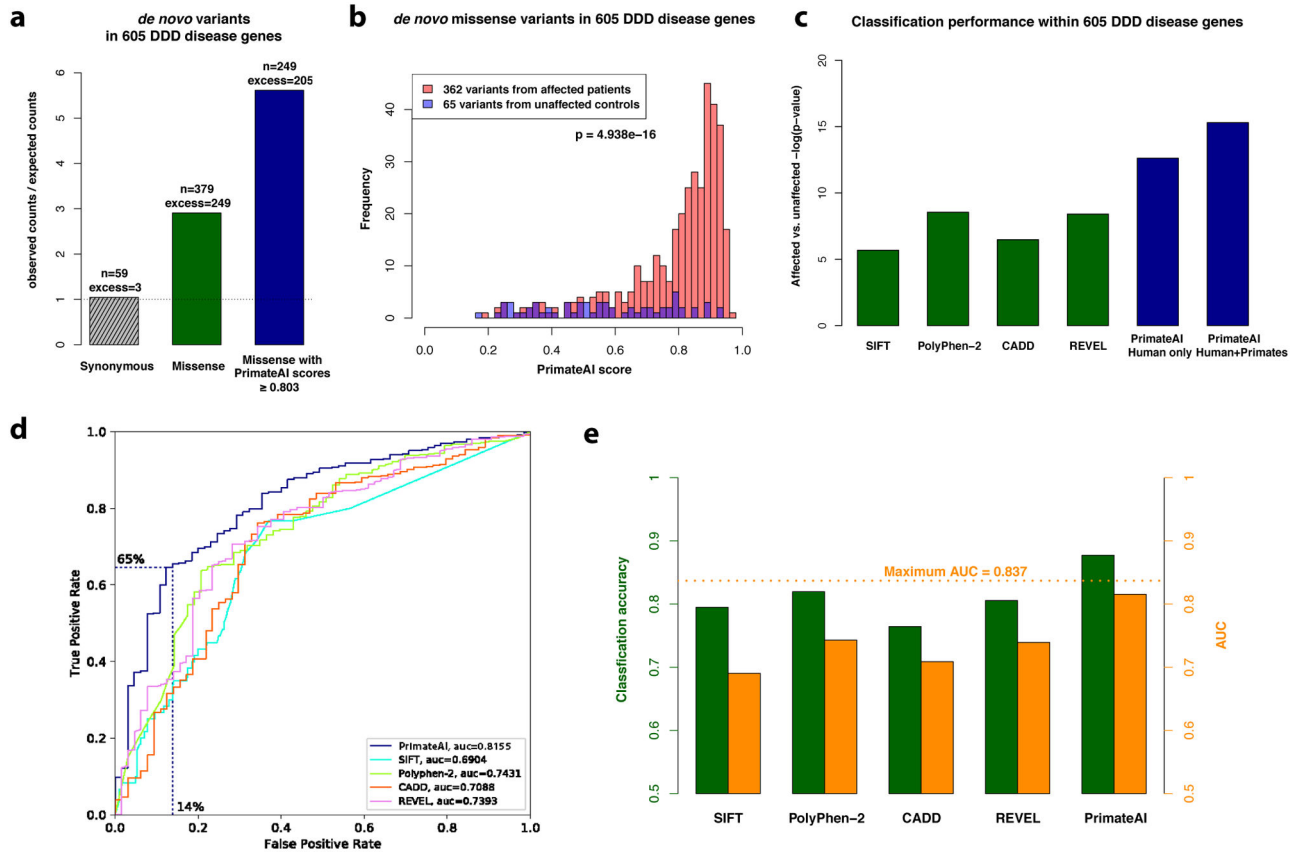
Figure 4. Classification accuracy within 605 DDD genes with P < 0.05

a, Enrichment of *de novo* missense mutations over expectation in affected individuals from the DDD cohort within 605 associated genes that were significant for *de novo* protein truncating variation (p<0.05). **b**, Distributions of PrimateAI prediction scores for *de novo* missense variants occurring in DDD patients vs unaffected siblings within the 605 associated genes, with corresponding Wilcoxon rank-sum p-value. **c**, Comparison of various classifiers at separating *de novo* missense variants in cases vs controls within the 605 genes. The y-axis shows the p-values of the Wilcoxon rank-sum test for each classifier. **d**, Comparison of various classifiers, shown on a Receiver Operator Characteristic (ROC) curve, with area under the curve (AUC) indicated for each classifier. **e**, Classification accuracy and AUC for each classifier. The classification accuracy shown is the average of the true positive and true negative error rates, using the threshold where the classifier would predict the same number of pathogenic and benign variants as expected based on the enrichment in Fig. 4a. To take into account that 33% of the DDD *de novo* missense variants represent background, the maximum achievable AUC for a perfect classifier is indicated with a dotted line.
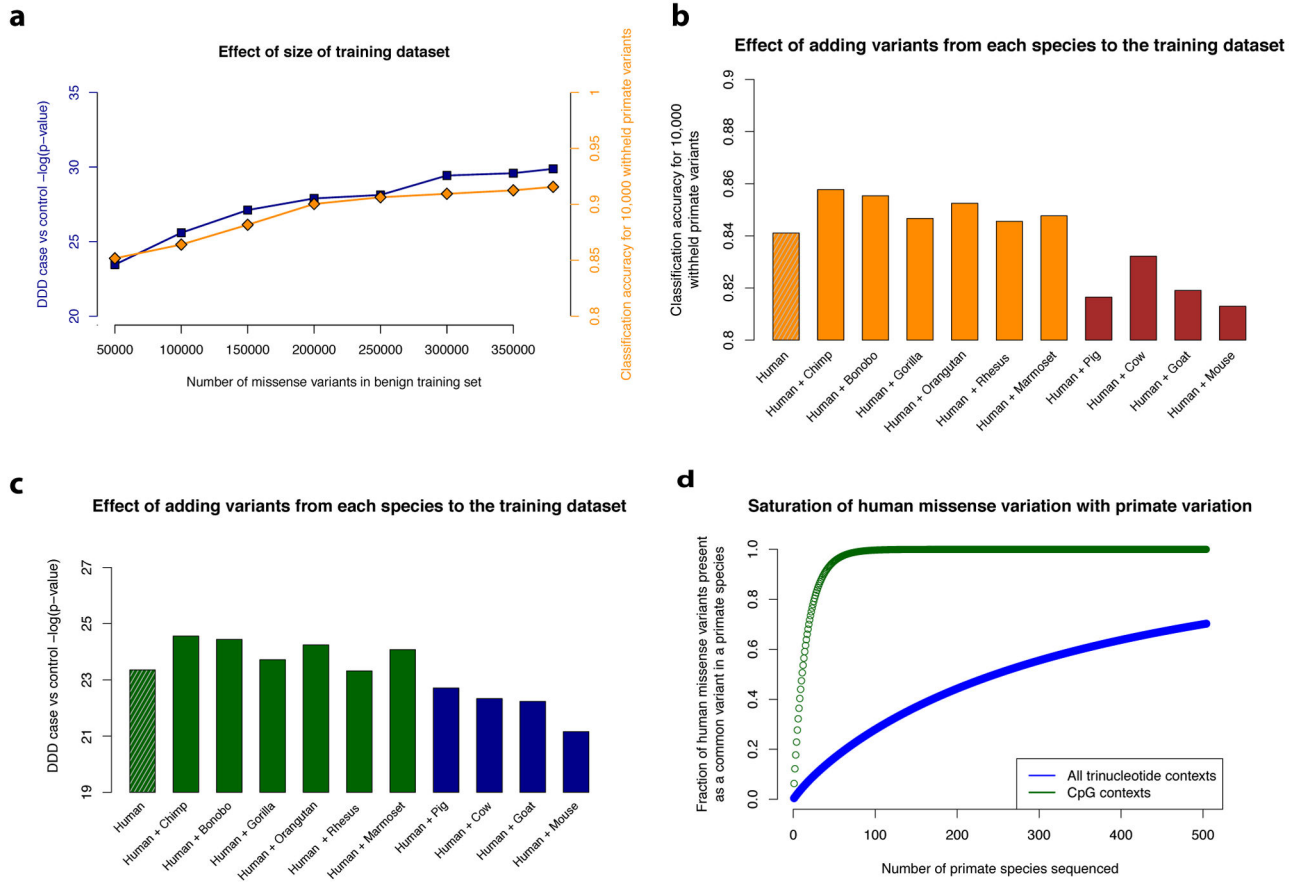
Figure 5. Impact of data used for training on classification accuracy

a, Deep learning networks trained with increasing numbers of primate and human common variants up to the full dataset (385,236 variants). Classification performance for each of the networks is benchmarked on accuracy for the 10,000 withheld primate variants (as in Fig. 3d) and *de novo* variants in DDD cases vs controls (as in Fig. 3f). **b–c**, Performance of networks trained using datasets consisting of 83,546 human common variants plus 23,380 variants from a single primate or mammal species. Results are shown for each network trained with different sources of common variation, **b,** benchmarked on 10,000 withheld primate variants, and **c**, on *de novo* missense variants in DDD cases vs controls. **d**, Expected saturation of all possible human benign missense positions by identical-by-state common variants (> 0.1%) in the 504 extant primate species. The y-axis shows the fraction of human missense variants observed in at least one primate species, with CpG missense variants indicated in red, and all missense variants indicated in blue. To simulate the common variants in each primate species, we sampled from the set of all possible single nucleotide substitutions with replacement, matching the trinucleotide context distribution observed for common human variants (> 0.1% allele frequency) in ExAC.

Table 1

Additional genes achieving genome-wide significance in intellectual disability when considering only missense *de novo* mutations (DNMs) with PrimateAI scores ≥ 0.803

Counts of protein truncating and missense DNMs are provided. P-values for gene enrichment are shown when the statistical test was run only with missense mutations with PrimateAI score ≥ 0.803, and when it was repeated for all missense mutations.

HGNC symbol	Protein-truncating variants	Missense		P-value		Phenotypic abnormalities observed in multiple individuals
		PrimateAI score ≥0.803	All missense	PrimateAI score ≥0.803	All missense	
ACTL6B	0	3	3	1.5×10^{-7}	2.4×10^{-6}	Microcephaly
EBF3	3	3	3	5.2×10^{-8}	5.4×10^{-6}	Growth delay, eye abnormality, strabismus, ataxia
EFTUD2	2	4	4	1.5×10^{-7}	1.5×10^{-5}	Microcephaly, low-set ears, microtia, choanal atresia
HECW2	1	8	8	2.8×10^{-10}	6.7×10^{-7}	Seizures, myopathy, abnormal calvarium
KDM6A	2	3	3	2.3×10^{-7}	9.8×10^{-6}	Eyelid, dental abnormalities, hypotonia
KIF5C	0	3	3	3.0×10^{-7}	2.8×10^{-6}	Cerebral hypoplasia
MAP2K1	0	5	5	3.1×10^{-8}	2.7×10^{-6}	Hypertelorism, low-set ears, polyhydramnois
PPP1CB	0	6	6	1.5×10^{-8}	1.6×10^{-6}	Abnormality of the forehead, short stature
PRKD1	0	6	6	8.6×10^{-8}	1.7×10^{-5}	Skin, digital, and cardiac abnormalities; sparse hair
SOX11	1	3	3	3.1×10^{-7}	2.4×10^{-5}	Hypermetropia, nail hypoplasia
TBR1	4	4	4	1.3×10^{-10}	4.2×10^{-7}	Autistic behavior
TLK2	3	5	5	4.7×10^{-9}	6.3×10^{-7}	Nose, eyelid abnormalities, slanted palpebral fissure
TRIP12	6	2	4	1.4×10^{-7}	5.4×10^{-7}	Joint laxity
U2AF2	0	4	4	2.6×10^{-7}	1.2×10^{-5}	Seizures; eye, palatal, philtrum abnormalities

Table 2

Comparison of the difference in Grantham score, Protein surface-exposure, and Amino acid sequence conservation between human expert annotated variants in ClinVar and *de novo* variants in DDD cases vs controls

Mean scores are shown for missense mutations with non-conflicting annotations in the ClinVar database, and for *de novo* variants present in DDD cases vs controls within 605 disease-associated genes. Protein surface-exposure reflects the fraction of amino acids predicted as exposed residues by the solvent accessibility neural network, and sequence conservation shows the fraction of amino acids with sequence identity in the 100-vertebrate alignment.

	Grantham score	Protein surface-exposed	Sequence conservation
ClinVar Pathogenic variants	91.1	.53	.87
ClinVar Benign variants	67.4	.41	.54
Difference in human-expert annotations	**+23.7**	+.12	**+.33**
de novo variants in DDD patients	84.9	.51	.90
de novo variants in healthy controls	72.7	.29	.73
Difference in affected vs unaffected individuals	+12.2	**+.22**	+.17